Journal of Power Sources 307 (2016) 435–442

Contents lists available at ScienceDirect

Journal of Power Sources

journal homepage: www.elsevier.com/locate/jpowsour

In situ lithiated FeF_3/C nanocomposite as high energy conversion-reaction cathode for lithium-ion batteries

Xiulin Fan [a], Yujie Zhu [a], Chao Luo [a], Tao Gao [a], Liumin Suo [a], Sz-Chian Liou [b], Kang Xu [c], Chunsheng Wang [a, *]

[a] Department of Chemical and Biomolecular Engineering, University of Maryland, College Park, MD 20742, USA
[b] Maryland Nanocenter, University of Maryland, College Park, MD 20742, USA
[c] Electrochemistry Branch, Power and Energy Division Sensor and Electron Devices Directorate, U.S. Army Research Laboratory, Adelphi, MD 20783, USA

HIGHLIGHTS

- Pre-lithiated FeF_3/C cathode with built-in Li source is *in situ* fabricated.
- Uniformly distributed Fe and LiF with size ~6 nm in carbon matrix are obtained.
- The cathode shows a superior performance with a high capacity of >400 mA h g^{-1}.
- A reversible discharge energy density of ~800 W h kg^{-1} is achieved.
- The prelithiated cathode can couple with the commercial lithium free anode.

GRAPHICAL ABSTRACT

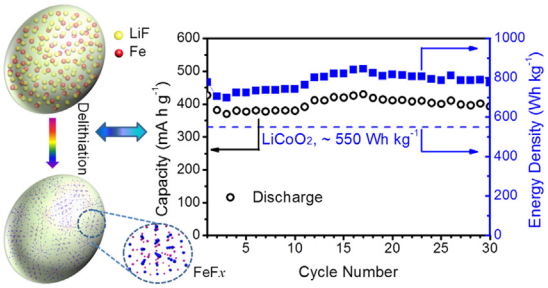

ARTICLE INFO

Article history:
Received 22 October 2015
Received in revised form
13 December 2015
Accepted 1 January 2016
Available online 12 January 2016

Keywords:
Lithium-ion battery
Conversion reaction
Iron fluoride
Cathode material
Prelithiation

ABSTRACT

Transition metal fluorides (such as FeF_3 and FeF_2) based on conversion chemistry have been considered as a promising alternative to the intercalation cathode materials due to the high capacity and high energy density. However, the critical challenges for these materials come from the absence of Li source in them, and low power density and poor cycling stability. Herein, pre-lithiated FeF_3 with extremely small size of Fe and LiF nanoparticles (both ~6 nm) homogeneously embedded in the carbon matrix were synthesized using a facile and scalable *in situ* strategy. Benefited from the ultra-small Fe and LiF nanoparticles, uniform distribution, and intimate contact between the active species and the carbon matrix, the particle-to-particle interfacial resistance and diffusion length for Li and F are dramatically reduced. As a result, a high specific capacity of over 400 mA h g^{-1} with a discharge energy density of ~700 W h kg^{-1} and favorable cycling performance are achieved, making such composite a promising high-capacity cathode for LIBs. Furthermore, the built-in Li source in this composite renders it a drop-in replacement for cathode materials used in the current LIB configurations, thus paving the way for the practical applications in the next generation of high energy density LIBs.

1. Introduction

Li ion batteries (LIBs) have been the exclusive power source for portable electronics since two decades ago, while their penetration into markets of more strategic importance such as vehicle

* Corresponding author.
E-mail address: cswang@umd.edu (C. Wang).

http://dx.doi.org/10.1016/j.jpowsour.2016.01.004
0378-7753/

electrification and grid storage has been hindered by their moderate energy densities, mainly due to the limits imposed by the intercalation-type cathode materials. These intrinsic limits come from the masses of inert framework, which serves as stationary lattice to accommodate the topotactic intercalation of Li^+, with the typical ratio of one Li per transition metal core [1]. While the framework does ensure the cell chemistry reversibility, it also simultaneously reduces the percentage of the effective mass (Li^+) that participates the electrochemical reactions. To breakthrough these limits, the concept of conversion-reaction materials was proposed [2,3], which is capable of accommodating more than one Li^+ per transition metal core in their reaction with Li:

$$MX_n + nLi^+ + ne \rightleftharpoons nLiX + M \quad (1)$$

(M = Fe, Cu, or Co, *etc*; X = ½S^{2-}, ½O^{2-}, or F^-, and n = 2 or 3 *etc*)

Such materials promise theoretical capacities well beyond what intercalation chemistry could compete. Among the diversified candidates investigated, transition metal fluorides MF_n attract most of the attention due to their higher specific capacities, and higher electrochemical potentials, all being resulted from the higher ionicity of M–F bonds and lower molecular weight of F than their oxide and sulfide counterparts. In particular, iron (III) fluoride (FeF_3) shows the highest theoretical capacity of 712 mA h g^{-1} (assuming a complete lithiation involving 3 electron transfer) at an average potential of ~2.74 V [4], potentially enabling a high theoretical energy density of 1951 W h kg^{-1} [3], which in combination with the low cost and environmental amity of iron, makes it most ideal battery chemistry for large scale applications of electric vehicles and grid storage [5].

It is believed that the lithiation of FeF_3 experiences stages of insertion and phase conversion reactions:

$$FeF_3 + Li^+ + e^- \leftrightarrow LiFeF_3 \quad (2)$$

$$LiFeF_3 + 2Li^+ + 2e^- \leftrightarrow LiF + Fe^0 \quad (3)$$

In the insertion reaction occurring at about 3.4 V, $Li_{0.5}FeF_3$ is first formed with a rutile-like structure [6], and then transformed to $LiFeF_3$ upon continuous lithiation, providing a theoretical capacity of 237 mA h g^{-1}. In the initial stage of insertion reaction, Li ions are accommodated in the interstitial sites of FeF_3 lattice, with the resultant Li_xFeF_3 still maintaining the original FeF_3 structure with a slight lattice expansion. At lower potential (~2.0 V), however, a phase change eventually occurs when more Li^+ is introduced into the lattice, turning $LiFeF_3$ into α-Fe^0 and LiF while providing an overall capacity of 712 mA h g^{-1} that involves a 3-electron transfer (Equation (2) and (3)) [7]. Since the electrode structure in conversion reaction processes experience breaking and reformation during each lithiation/de-lithiation cycle, the reversibility has been the universal challenge for this class of cathode chemistries, as reflected by the low Coulombic efficiencies in the first conversion cycle when the fluorides react with Li, low energy efficiency due to the severe polarization between charging and discharging, as well as rapid capacity fading. Volume expansion caused by the inclusion of Li into the conversion-reaction adds more irreversibility as electrode pulverization always leads to loss of active materials. Therefore, in previous studies only a dozen cycles can be achieved with a capacity of <210 mA h g^{-1} [8–10]. Poor cycling stability, usually with less than 20 cycles, always ensues when a full conversion reaction turning $LiFeF_3$ into α-Fe and LiF from 4.2 V to 1.5 V is involved [11–14], For example, ball milled FeF_3/C composite could only be charged/discharged at a very low current of 7.58 mA g^{-1} at 70 °C, and the capacity of 600 mA h g^{-1} quickly faded within 14 cycles [15]. By limiting the cycle potential of FeF_3 in the insertion reaction range, better cycling stability was achieved, with the compromise in capacity [10,11,16].

In addition to poor cycling stability, FeF_3 cathodes also show large potential hysteresis (0.5–1.5 V) between lithiation and delithiation due to sluggish lithiation/delithiation kinetics, especially for the second step [7,17], which is attributed to different pathways between lithiation and delithiation [14], and high stress/strain induced by large volume change. Nanotechnologies have been used to overcome this barrier by designing and synthesizing FeF_3/C nanocomposites so that Li^+ diffusion distance could be shortened to nanometric scale. High-energy ball-milling [15,18], HF-based aqueous solution synthesis [9,19,20], solid–liquid reaction [21,22], ionic liquid assistant synthesis method [16,23,24] as well as physical vapor deposition have been applied [25], however with only limited success in reducing the potential hysteresis.

Another challenge little discussed thus far but nonetheless critical to practical manufacturing is that the majority of conversion-reaction cathode materials do not carry built-in Li source. FeF_3 cannot be coupled with the present non-lithiated anode such as graphite or silicon [26,27]. To couple the present non-lithiated anode, LiF–Fe^0 composite in which two components must be well-dispersed and in intimate contact with each other is required to form FeF_3 upon delithiation. The conversion-reaction within such a pre-lithiated composite should proceed with the charge (de-lithiation) process as the initial step, as what happens in all Li-ion batteries. Composite materials thus constructed would require no extra Li source at cell building, and electrode pulverization caused by volume expansion should be reduced as Li already occupies its position in the composite. Unfortunately, attempts to construct such lithiated composite using conventional ball milling and pyrolysis technologies showed even inferior electrochemical performance due to the inhomogeneity of structure and composition. For example, a low capacity of ~160 mA h g^{-1} was obtained from a LiF/Fe/Graphene nanocomposite [28], and of 230 mA h g^{-1} from Fe/LiF/C composite [29]. In particular, the distinct hysteresis during the first and the subsequent cycles in all the above cases highlight the difficulty in interfacing LiF with the active storage sites (Fe^0). The combined effect of the above challenges is responsible for keeping conversion-reaction materials a lab curiosity thus far.

In the present work, we successfully resolved these challenges arising from conversion-reaction chemistry of FeF_3. Through a chemical ball-milling process, LiF and Fe nanoparticles (~6 nm) were evenly dispersed in nano-scale in a carbon matrix as the lithiated precursor of FeF_3. This lithiated conversion-reaction nanocomposite (Fe/LiF/C), different from most conversion-reaction materials investigated thus far but similar to the cathode materials that have been used for Li-ion industry, exhibits exceptional electrochemical reversibility, delivering a reversible capacity as high as >400 mA h g^{-1} at the room temperature for over 30 cycles. Detailed characterizations reveal that Fe and LiF nanoparticles of extremely small sizes (~6 nm) are homogenously dispersed in the carbon matrix, and form iron fluoride reversibly upon delithiation (charging). The above performance improvements as well as understanding of electrochemical reaction mechanism of the lithiated conversion-reaction composite represent a significant advance for the efforts in designing practical cathode materials for the next generation batteries.

2. Experimental section

2.1. Materials

Anhydrous FeF_3 (98%, Aldrich), LiH (powder, ~30 mesh, 95%), were purchased from Sigma–Aldrich and used as received. Fe

(powder, <10 μm, >99.9%) LiF (powder, >99%) were purchased from Alfa-Aesar.

2.2. Synthesis of the Fe/LiF/C composite

Fe/LiF/C nanocomposites were synthesized by reactive ball milling. First, FeF_3 (Anhydrous, 98%, Aldrich) and carbon black (75:25 in weight ratio) were pre-milled for 5 h to get a well distributed FeF_3/C composite. LiH (95%, Aldrich) and carbon black (75:25 in weight ratio) were pre-milled for 10 h to get a well-distributed LiH/C composite. Then, the pre-milled FeF_3/C and LiH/C (1:3 in mole ratio) were combined and further ball-milled for 12 h at 500 rpm to get the Fe/LiF/C composite. As reference for comparison, we also synthesized Fe/LiF/C composite using the commercial Fe, LiF and carbon black as the starting materials following the same procedure.

2.3. Material characterizations

Scanning electron microscopy (SEM) and transmission electron microscopy (TEM) images were taken by Hitachi SU-70 analytical SEM (Japan) and JEOL 2100F equipped with field emission gun (Japan) and Gatan image filter (Tridium 863), respectively. X-ray diffraction (XRD) pattern was recorded by Bruker Smart1000 (Bruker AXS Inc., USA) using Cu Kα radiation.

The electrochemical tests were performed using a coin-type half cell (CR 2032). Metallic lithium was used as the negative electrode. To prepare working electrode, the as-synthesized Fe/LiF/C nanocomposite, carbon black, and PVDF with mass ratio 70:15:15 were mixed into homogeneous slurry in NMP with pestle and mortar. The slurry mixture was coated onto Al foil and then dried at 100 °C for 12 h. To avoid the possible contamination from oxygen and moisture, the electrode preparation and the drying process were performed in the glovebox. The loading mass of the active materials for the electrode is about 0.2 mg/cm^2. The electrolyte solution comprised of 1 M $LiPF_6$ in fluoroethylene carbonate (FEC)/2-fluoroethyl methyl carbonate (FEMC)/hydrofluoroether (HFE) (2:6:2 by volume). The cells were assembled with a polypropylene (PP) microporous film (Celgard 3501) as the separator. Electrochemical performance was tested using Arbin battery test station (BT2000, Arbin Instruments, USA). Capacity was calculated on the basis of the mass of active species. Cyclic voltammogram scanned at 0.1 mV/s between 1.2 and 4.5 V was recorded using a CHI 600E electrochemical workstation (CH Instruments Inc. USA).

3. Results and discussion

3.1. Synthesis and characterization

Upon close examination of the previous studies, we believe that the low capacities accessed in these pre-lithiated Fe/LiF/C composites (<300 mA h g^{-1}), which are far less than the capacity of corresponding non-lithiated FeF_3/C materials, are mainly caused by the high interfacial impedance and long Li^+-diffusion pathway due to large particle size of Fe and poor contact between Fe and LiF species. The minimum Fe particle size reported in LiF/Fe composites synthesized using state-of-art technologies is about 20 nm [26,28,30], which is still much larger than the average size of transition metal nanoparticles (~6 nm) formed by *in situ* electrochemical reduction of non-lithiated metal fluorides [17,31]. In this work, we attempt to form Fe and LiF nanoparticles with average size of ~6 nm and uniformly disperse them in a carbon matrix by using chemical ball milling, in which FeF_3 is *in situ* reduced into Fe/LiF nanocomposite to ensure the intimate contact between the active species (Fe and LiF) in the resultant Fe/LiF/C nanocomposite. Fig. 1 schematically shows this fabrication process, with a detailed description given in the Experimental section. Nanocomposites of FeF_3/C and lithiating agent LiH/C were first fabricated by ball-milling FeF_3 and LiH with carbon black separately. During this "mechanical" ball milling process, both FeF_3 and LiH were well fragmented into nanometer size [18], resulting in a well dispersed FeF_3/C or LiH/C nanocomposites. A "chemical" ball-milling was then adopted by ball-milling the FeF_3/C and LiH/C nanocomposites together to *in situ* generate Fe/LiF/C nanocomposite through reaction 4:

$$3LiH + FeF_3 \rightarrow 3LiF + Fe + 1.5H_2\uparrow \quad \Delta G_f = -588\ \text{kJ mol}^{-1} \qquad (4)$$

The LiF/Fe/C nanocomposite synthesized from chemical reaction between nano-LiH and nano-FeF_3 possesses similar structure and particle size as those formed electrochemically *via* the lithiation of FeF_3. In particular, the sizes of Fe and LiF are much smaller and more narrowly distributed than those formed *via* traditional mechanical ball-milling the mixture of Fe and LiF. Such difference should be attributed to the high strength and its resistance to fragmentation into nanometer size of Fe in the traditionally mechanical ball milling process, but the fragile and brittle nature of both FeF_3 and LiH [19] in mechanical and subsequent chemical ball-milling processes can accelerate the pulverization to form nano-Fe and LiF. Also contributing to the nanocomposite is the ductile nature of carbon black, which can easily be deformed into lamellae along the (002) planes during ball-powder-ball collisions [32], and consequently hinders the over-growth of the Fe and LiF nanoparticles formed *in situ*, resulting in the extremely small sizes for both components.

The crystal structure and morphology of the *in situ* synthesized Fe/LiF/C composite were characterized by X-ray diffraction (XRD), scanning electron microscopy (SEM) and transmission electron microscopy (TEM) analyses. All diffraction peaks in the XRD patterns (Fig. 2) can be assigned to Fe (cubic, *Im-3m*, PDF#06-0696) and LiF (cubic, *Fm-3m*, PDF#45-1460). No impurities can be detected, implying that FeF_3 and LiH were completely converted into Fe and LiF. Compared to the sharp peaks of Fe and LiF in Fe/LiF/C nanocomposite synthesized from traditionally top–down mechanical ball-milling of mixture of commercial Fe, LiF and carbon black, the Fe and LiF in Fe/LiF/C nanocomposite from bottom-up chemical ball-milling show very broadened and weak diffraction peaks, suggesting that the Fe and LiF formed *in situ via* chemical ball-milling are indeed nanocrystalline or even disordered. Using Scherrer equation ($d = 0.9\lambda/\beta\cos\theta$), the average grain size of LiF and Fe is estimated about 9.7 and 6.2 nm, respectively. SEM images in Fig. 3a and b reveal that the primary Fe/LiF/C particles with size of ~30 nm agglomerate into micro-sized secondary particles. The energy-dispersive spectroscopy (EDS) elemental mapping (Fig. S1) of micro-sized aggregated secondary particles confirms the homogeneous distribution of Fe, F, and C in the chemically ball-milled Fe/LiF/C nanocomposites, where the colors of three elements are overlapped uniformly. In contrast, Fe particles as large as 2 μm can still be observed in the Fe/LiF/C composite synthesized *via* conventionally mechanical ball milling the mixture of commercial Fe, LiF and carbon black (Fig. S2), which agrees well with the intensive diffraction peaks for this composite (Fig. 2).

The selected-area electron diffraction (SAED) patterns of chemically ball-milled LiF/Fe/C nanocomposites in TEM (Fig. S3) reveal the existence of Fe and LiF nanograins, whose diffuse rings indicate that the crystalline sizes of Fe and LiF are rather small, in accordance with the broad peaks of XRD patterns. The magnified TEM images shown in Fig. 3c–e clearly show that one composite primary particle is composed of multiple nanocrystalline domains with a diameter less than 6 nm. The nano-domains with darkest

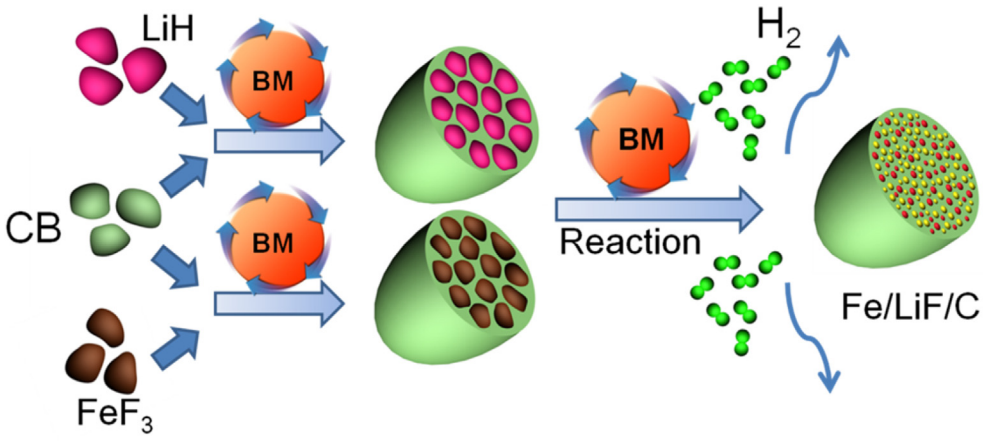

Fig. 1. Schematic illustration of the preparation of Fe/LiF/C nanocomposite *via* mechanical and chemical ball-milling. BM and CB stand for ball milling and carbon black, respectively.

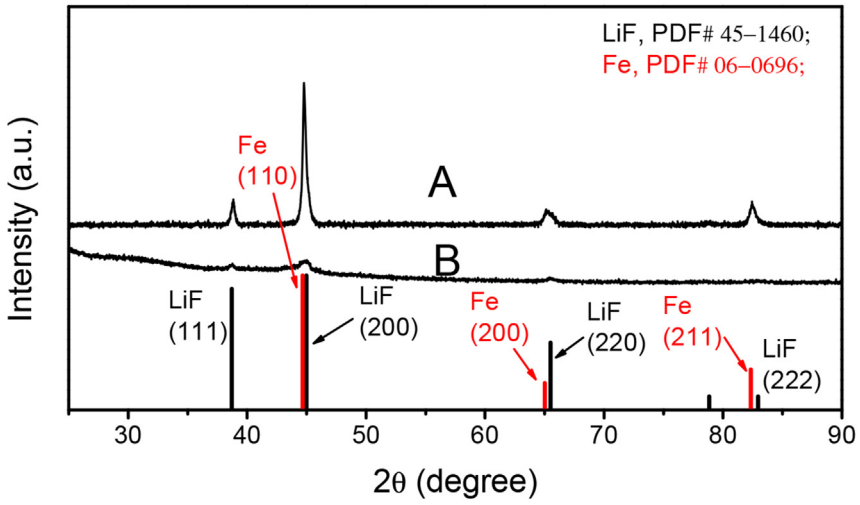

Fig. 2. XRD patterns for the Fe/LiF/C composite synthesized by traditionally mechanical ball milling of commercial Fe, LiF and carbon black (A); and Fe/LiF/C composite synthesized by chemical ball milling of the nano-FeF_3/C, nano-LiH/C (B).

contrast can be indexed to Fe, while the nano-clusters with little bright color can be referred to the LiF in the carbon matrix, because the latter is less visible than the transition metal domains due to the weak scattering of light constituent elements (lower atomic number elements) in the bright field images during TEM image formation [31]. HRTEM image and fast Fourier transform (FFT) analysis for the dark nanoclusters in the composite are shown in Fig. 3f. Lattice fringes with a spacing of 0.2 nm can be seen for the nanoparticle, corresponding to the (110) planes of metallic iron (cubic, Im-3m). Distinct graphite layers can be clearly observed outside the composite nanoparticles (Fig. 3d), corresponding to the undestroyed (002) planes of the graphic grain. These carbon layers together with the carbon matrix can function as the ion and electron transport channels and as well as a mechanical buffer to accommodate the volume changes during the charging–discharging processes. All composite particles exhibit the similar structures (Fig. S4) where the Fe and LiF nanoclusters are uniformly dispersed in the carbon matrix. Based on these TEM images, histogram of particle size distribution was obtained (as shown in Fig. S5), which confirmed the homogeneous distribution of *in situ* formed Fe and LiF in the composite, and was in good agreement with the XRD results. Such uniform distribution of Fe and LiF generated *in situ* with extremely small size ensures perfect physical contact between the active Fe and LiF nanoparticles, thus significantly reducing the interfacial impedance. Since a complete conversion reaction not only involves the Li transport but also requires the migration of much heavier ions (F^-) in the nanocomposite, the extremely small sizes of these Fe and LiF nanoparticles could significantly shorten the diffusion distances for all ions participating in the electrochemical reactions.

3.2. Electrochemical performance

The electrochemical performance of the *in situ* synthesized Fe/LiF/C composite was investigated in 1 M $LiPF_6$ in FEC/FEMC/HFE (2:6:2) by cyclic voltammetry (CV) and galvanostatic charge/discharge cycling. As shown in Fig. S6 with three different electrolyte compositions frequently used, EC or DMC apparently can not withstand the oxidative decomposition during the initial charging process due to the high catalytic activity of nano-sized Fe. Therefore, more oxidatively stable FEC, FEMC, and HFE solvents were used. Fig. 4a shows the CV profiles of chemically ball-milled Fe/LiF/C composite after 5th pre-activation cycles at a scanning rate of 0.1 mV s^{-1}. During the cathodic/anodic reaction, two large peaks can be observed in each reaction. The cathodic peak around 3.0 V and the corresponding anodic peak of 3.4 V are attributed to

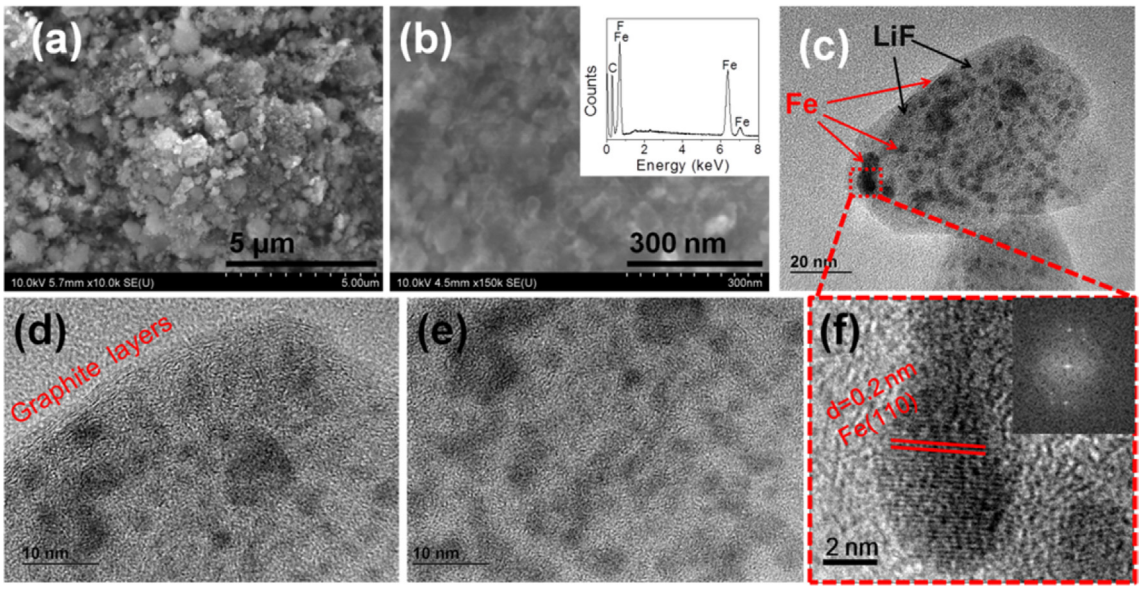

Fig. 3. (a) and (b) the SEM images of the *in situ* synthesized Fe/LiF/C composite; (c), (d) and (e) the TEM and HRTEM images of the chemically ball-milled Fe/LiF/C composite. (f) The magnified HRTEM image of the dark nanoparticle in figure (c). The inset of figure (b) is the EDS spectra of the composite. The inset of figure (f) is the corresponding FFT image of dark nanoparticle.

the de-intercalation/intercalation of FeF_3 (Equation (2)), while the cathodic peak near 1.7 V and the corresponding anodic peak near 3.0 V are related to conversion reaction (Equation (3)). The potential difference between the cathodic and anodic peaks of Equations (2) and (3) at a scan rate of 0.1 mV s^{-1} are about 0.4 V and 1.3 V, respectively. The over-potential and potential hysteresis are related to the large energy barrier for the formation/dissociation of the LiF and the transport of the heavier ions during charging/discharging processes [13,33]. From 5th to 9th cycles after activation, the current densities are slightly increased, indicating the slight capacity increase during cycling.

Fig. 4b shows the galvanostatic discharge/charge curves of chemically ball-milled Fe/LiF/C nanocomposite at a constant current density of 25 mA g^{-1} at 25 °C. Both the lithiation and delithiation capacities increase as change/discharge cycling proceeds, demonstrating that an activation process is needed to extract lithium from Fe/LiF/C nanocomposite. The first charge capacity of chemically ball-milled Fe/LiFe/C nanocomposites is 316 mA h g^{-1} with coulombic efficiency of 75%. To our best knowledge, it is the highest initial charge capacity and coulombic efficiency reported for all pre-lithiated metal fluoride cathode materials [26,28,30,34]. Upon further charge/discharge cycles, the capacity gradually increased and stabilized around 390–410 mA h g^{-1} after the 20th cycle (Fig. 4c), demonstrating one of the best performance among all iron fluoride conversion-reaction composites reported either pre-lithiated or unlithiated [11,23,35,36]. The discharge profiles clearly show two voltage plateaus. The capacity in the high voltage plateau from 4.0 V to 2.4 V, corresponding to the lithium intercalation to FeF_3 and formation of $LiFeF_3$ [13,14,22,35], dramatically increased from about 50 mA h g^{-1} in the first discharge to ~100 mA h g^{-1} in the 20th discharge. A longer high-voltage plateau indicates the higher FeF_3 percentage for the charged composite. Although slight capacity decay can be observed for longer cycles, a reversible capacity of about 300 mA h g^{-1} can still be achieved after 50^{th} cycle. The slight fluctuation of the capacity was caused by the variation of room temperatures during cycling, as the kinetics of conversion materials has been known to be temperature-sensitive [22]. For the mechanically ball-milled Fe/LiF/C nanocomposite, very small high-voltage plateau with capacity of only 20 mA h g^{-1} can be observed during discharge, as shown in Fig. S5. The low voltage plateau below 2.0 V in Fig. 4b is associated with the conversion reaction of $LiFeF_3$ (or FeF_2) to Fe and LiF, the detailed mechanism will be discussed in the following section. The two plateau regions in galvanostatic discharge/charge curves are in accordance with the two peaks in CV profiles during lithiation/delithiation scanning of the materials (Fig. 4a). Fig. S6 shows the charge–discharge curves at varied current densities. A reversible capacity of over 150 mA h g^{-1} can be achieved at a high current of 100 mA g^{-1}.

Although the average potential of chemically ball-milled Fe/LiF/C nanocomposite is lower than commercial $LiCoO_2$ cathodes, its more than twice higher capacity than $LiCoO_2$ (140 mA h g^{-1}) renders a higher energy density of over 700 W h kg^{-1}, which is much higher than theoretical energy density of $LiCoO_2$ (550 W h kg^{-1}) (Fig. 4d). To the best of our knowledge, such superior electrochemical performance for the pre-lithiated fluoride materials has never been reported before [28–30,34,37]. Table S1 and S2 compile the representative electrochemical performance for the non-lithiated and lithiated fluorides materials, respectively, which clearly show that chemically ball-milled Fe/LiF/C possesses the best overall electrochemical performance in term of energy density and cycling stability among all fluoride and prelithiated fluoride cathodes reported. As comparison, Fe/LiF/C composite prepared *via* mechanical ball milling method only shows an initial charged capacity of 60 mA h g^{-1}, which increases to ~100 mA h g^{-1} during the initial 20 cycles and then fades to 80 mA h g^{-1} at the 30th cycles (Fig. S5).

The high electrochemical reversibility and capacity utilization of chemically ball-milled Fe/LiF/C nanocomposite can probably be attributed to the homogeneous distribution of ultra-small Fe and LiF (~6 nm) nanoparticles in the carbon matrix, which is comparable to or even better than the Fe/LiF/C nanocomposite generated during *in situ* electrochemical lithiation of FeF_3 process (Table S1). These ultra-small Fe and LiF nanoparticles entangled intimately in the carbon matrix, which not only significantly enhances the effective electrical conductivity, but also provides percolating transport paths for the Li^+ and F^- ions, hence reducing the particle-

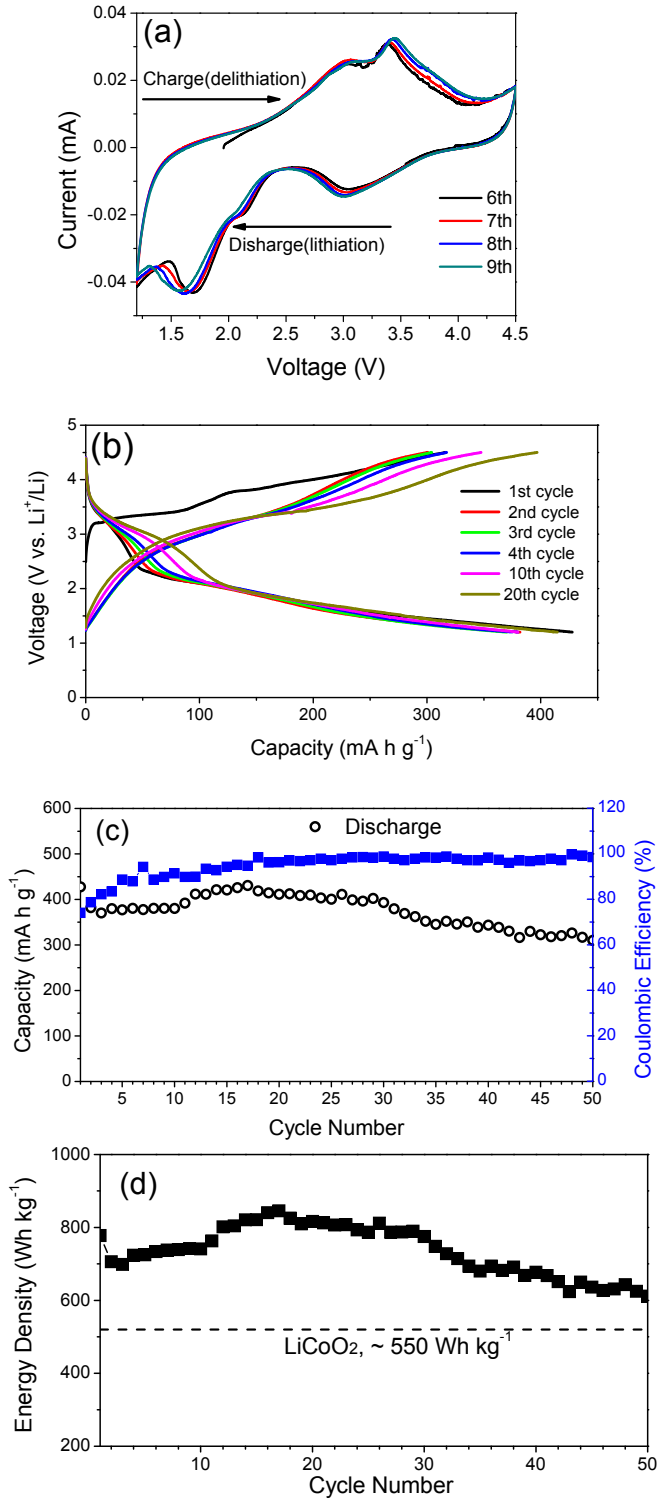

Fig. 4. (a) Cyclic voltammograms of chemically ball-milled Fe/LiF/C composite electrode scanned between 1.2 and 4.5 V at a rate of 0.1 mV S^{-1}; (b) Electrochemical charge/discharge curves of chemically ball-milled Fe/LiF/C composite at a constant current of 25 mA g^{-1} in the voltage window 1.2–4.5 V at room temperature; (c) Cycling performance of chemically ball-milled Fe/LiF/C composite at 25 mA g^{-1}. (d) Discharge energy density *vs.* cycle number along with the theoretical discharge energy density of $LiCoO_2$ cathode material (550 W h kg^{-1}).

to-particle interfacial resistance. As a comparison, the traditionally mechanical ball-milling failed to achieve those levels of nano-contacts, as characterized by a reversible capacity of less than 100 mA h g^{-1}. Unlike FeF_3 materials, the chemically ball-milled Fe/LiF/C nanocomposite is already in discharged state and contains Li-source. It could be coupled with non-lithiated anode materials that Li-ion industry is accustomed to. Since Li is already in the composite, the charging (delithiation) of Fe/LiF/C nanocomposite is accompanied with volume reduction, which circumvents the stress/strain in FeF_3 materials introduced by Li-inclusion in the first cycle. This feature would further enhance the mechanical integrity of the nanocomposite and lead to better cycling stability.

The thermodynamic potential hysteresis and kinetic overpotentials of chemically ball-milled Fe/LiF/C nanocomposites at different lithiation/delithiation levels were further investigated using galvanostatic intermittent titration technique (GITT) after the 5th cycle activation process. During GITT measurements, the electrode was charged/discharged at a pulse current of 40 mA g^{-1} for duration of 1.5 h, followed by a long relaxation of 20 h at open-circuit to obtain equilibrium potential. Fig. 5 shows the potential response during the GITT measurement for the chemically ball-milled Fe/LiF/C electrode, where the hollow dots represent the equilibrium open-circuit potential (OCP), while the complete profile for the delithiation and lithiation process along with the voltage relaxation during the open circuit periods is shown in Fig. S6. The thermodynamic potential hysteresis of Fe/LiF/C nanocomposite is found to be only 0.4–0.6 V, while the kinetic overpotential in lithiation is 0.1 V during intercalation process at 3.0 V but more than 0.7 V during conversion reaction process below 2.0 V for the delithiation conversion reaction. The overpotential gradually increases, probably due to the increasingly poor contact with carbon matrix because the delithiation reaction is a volume contraction process. The potential change during open-circuit is demonstrated in Fig. S6. During relaxation period in the initial charging and discharging process, the electrode seems to reach the equilibrium state rather quickly. With further lithiation/delithiation, it takes longer time for Fe/LiF/C nanocomposites to reach equilibrium potential, indicating slower diffusion and phase change reaction, especially near the end of the charge (at about 4.5 V) or end of discharge (at about 1.2 V). The gradually increased time to reach equilibrium potential and increased diffusion overpotential suggests that diffusion length of ions and/or phase change reaction resistance increase as conversion reaction proceeds.

The reversibility of conversion reaction was also investigated using XRD technique. Fig. 6 shows the XRD patterns for the chemically ball-milled Fe/LiF/C after charged to 4.5 V at a current of 10 mA g^{-1}. The fully delithiated Fe/LiF/C consists of FeF_2 and FeF_3, indicating an incomplete conversion reaction of the composite.

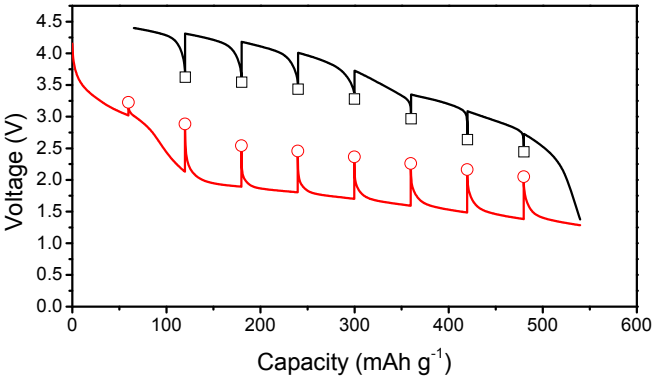

Fig. 5. Potential response of chemically ball milled Fe/LiF/C nanocomposite during GITT measurement. The hollow dots represent the equilibrium open-circuit potential (OCP).

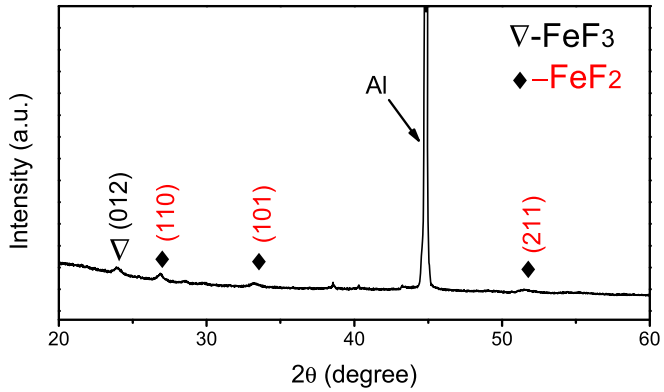

Fig. 6. XRD patterns for the Fe/LiF/C composite after 5th cycling charged to 4.5 V.

These results are in good agreement with the charge/discharge curves. The incomplete transformation from Fe/LiF to FeF_3 results in the variation of the capacity within the high voltage range (50–100 mA h g^{-1}) from the theoretical value of 237 mA h g^{-1}. Similar results are also observed for the non-lithiated FeF_3/C composite during the recharging process [15]. It is obvious that the FeF_3 conversion reaction not only involves the Li^+-transport but also the migration of much heavier atoms such as F^- or even Fe^{n+}. The detailed reaction mechanisms remain controversial because a series of intermediates may be formed during the reaction [8,14]. The nonequilibrium paths due to much faster diffusion of Li^+ than heavier ions result in the incomplete transformation of LiF/Fe to FeF_3 and form the rutile FeF_2-like structure [14].

The phase transformation of Fe/LiF/C composite after charged to 4.5 V was determined using SEM, Electron Energy Loss Spectroscopy (EELS) and TEM. Fig. S7 shows the SEM images for the composite after the 5th cycles. As expected, no cracks were observed, as Fe/LiF/C is in volume-expanded state. Since the intensity of STEM-HAADF (high-angle annular dark field) is proportional to $z^{1.7}$ (z is atomic number), the elements with different atomic number can be clearly observed in the STEM-HADDF mode. The STEM-HAADF image of the composite charged to 4.5 V is shown in Fig. 7a. The area with brighter contrast represents the heavier elements, which are Fe and F. Fig. 7b and c displays the EELS elemental mapping of Fe and F corresponding to the marked area shown in Fig. 7a. The elemental Fe and F are perfectly overlapped in the nanoparticles, indicating that the Fe and F are bonded and form a compound, which is consistent with the XRD results (Fig. 6). Fig. 7d shows the corresponding F *K*-edge and the Fe $L_{2,3}$-edge spectra, which reveals a similar feature with FeF_2. [22,38] Fig. 7e shows the HRTEM image for the charged composite. Crystalline nanoparticles with size of about 8 nm are uniformly distributed in the composite, some of which can be indexed to the FeF_2 species according to the distinct

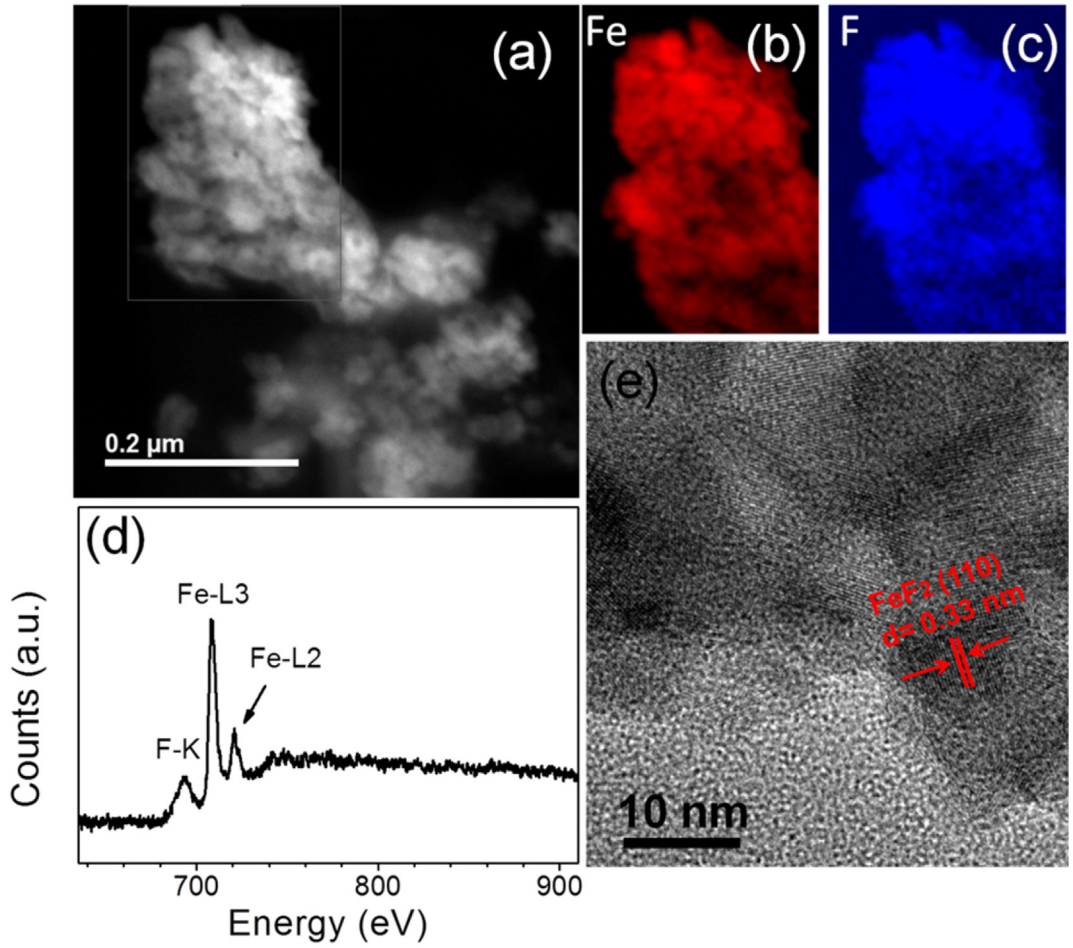

Fig. 7. (a) the HADDF-STEM image of Fe/LiF/C composite charged to 4.5 V at 10 mA g^{-1} after 5th charge/discharge cycles; (b) and (c) are the electron energy loss spectra (EELS) elemental mapping of Fe and F recorded for the area shown in figure (a); (d) the corresponding electron energy loss spectra for the area; (e) HRTEM image of Fe/LiF/C composite charged to 4.5 V after 5th charge/discharge cycles.

lattice d-spacing, as shown in Fig. 7e. FeF_3 is also present as demonstrated by XRD in Fig. 6 and discharge curves in Fig. 4b.

4. Conclusion

In summary, Fe/LiF/C hierarchical nanocomposites with LiF and Fe nanoparticles (~6 nm) uniformly dispersed in the carbon matrix were successfully synthesized *in situ* using chemically ball-milling method. This Fe/LiF/C nanocomposite cathode delivers a stable reversible capacity as high as >400 mA h g^{-1} with a high discharging energy density of over 700 W h g^{-1} at the room temperature. The significant improvement of the electrochemical performance is attributed to the combination of extremely small size of the Fe and LiF particles (~6 nm) and their intimate contact with carbon matrix, which enlarges the reaction area and reduces the diffusion length for Li, F and Fe. The pre-lithiated state of this cathode material together with the facile and scalable chemically ball-milling method could open up a novel avenue for the practical application of conversion cathode materials for lithium ion batteries.

Acknowledgments

This work was supported by Army Research Laboratory under Award Number W911NF1420031. The authors gratefully acknowledge the support of the Maryland NanoCenter and its NispLab. The highly pure fluorinated solvents were provided by Drs. Ron Hendershot and Joe Sundstrom of Daikin America.

Appendix A. Supplementary data

Supplementary data related to this article can be found at http://dx.doi.org/10.1016/j.jpowsour.2016.01.004.

References

[1] M.S. Whittingham, Chem. Rev. 114 (2014) 11414–11443.
[2] P. Poizot, S. Laruelle, S. Grugeon, L. Dupont, J.M. Tarascon, Nature 407 (2000) 496–499.
[3] G.G. Amatucci, N. Pereira, J. Fluor. Chem. 128 (2007) 243–262.
[4] H. Li, G. Richter, J. Maier, Adv. Mater. 15 (2003) 736–739.
[5] D. Andre, S.J. Kim, P. Lamp, S.F. Lux, F. Maglia, O. Paschos, B. Stiaszny, J. Mater. Chem. A 3 (2015) 6709–6732.
[6] S.K. Martha, J. Nanda, H. Zhou, J.C. Idrobo, N.J. Dudney, S. Pannala, S. Dai, J. Wang, P.V. Braun, RSC Adv. 4 (2014) 6730–6737.
[7] N. Yamakawa, M. Jiang, B. Key, C.P. Grey, J. Am. Chem. Soc. 131 (2009) 10525–10536.
[8] D. Ma, Z. Cao, H. Wang, X. Huang, L. Wang, X. Zhang, Energy Environ. Sci. 5 (2012) 8538–8542.
[9] L. Liu, M. Zhou, L. Yi, H. Guo, J. Tan, H. Shu, X. Yang, Z. Yang, X. Wang, J. Mater. Chem. 22 (2012) 17539–17550.
[10] N. Yabuuchi, M. Sugano, Y. Yamakawa, I. Nakai, K. Sakamoto, H. Muramatsu, S. Komaba, J. Mater. Chem. 21 (2011) 10035–10041.
[11] H.J. Tan, H.L. Smith, L. Kim, T.K. Harding, S.C. Jones, B. Fultz, J. Electrochem. Soc. 161 (2014) A445–A449.
[12] J.K. Ko, K.M. Wiaderek, N. Pereira, T.L. Kinnibrugh, J.R. Kim, P.J. Chupas, K.W. Chapman, G.G. Amatucci, Acs Appl. Mater. Inter. 6 (2014) 10858–10869.
[13] P. Liu, J.J. Vajo, J.S. Wang, W. Li, J. Liu, J. Phys. Chem. C 116 (2012) 6467–6473.
[14] R.E. Doe, K.A. Persson, Y.S. Meng, G. Ceder, Chem. Mater. 20 (2008) 5274–5283.
[15] F. Badway, F. Cosandey, N. Pereira, G.G. Amatucci, J. Electrochem. Soc. 150 (2003) A1318–A1327.
[16] (a) C. Li, X. Mu, P.A. van Aken, J. Maier, Adv. Energy Mater. 3 (2013) 113–119; (b) Y. Bai, X. Zhou, Z. Jia, C. Wu, L. Yang, M. Chen, H. Zhao, F. Wu, G. Liu, Nano Energy (2015), http://dx.doi.org/10.1016/j.nanoen.2015.08.006.
[17] F. Wang, R. Robert, N.A. Chernova, N. Pereira, F. Omenya, F. Badway, X. Hua, M. Ruotolo, R. Zhang, L. Wu, V. Volkov, D. Su, B. Key, M.S. Whittingham, C.P. Grey, G.G. Amatucci, Y. Zhu, J. Graetz, J. Am. Chem. Soc. 133 (2011) 18828–18836.
[18] F. Badway, N. Pereira, F. Cosandey, G.G. Amatucci, J. Electrochem. Soc. 150 (2003) A1209–A1218.
[19] S.W. Kim, D.H. Seo, H. Gwon, J. Kim, K. Kang, Adv. Mater. 22 (2010) 5260–5264.
[20] J. Liu, W. Liu, S. Ji, Y. Wan, M. Gu, H. Yin, Y. Zhou, Chem. Eur. J. 20 (2014) 5815–5820.
[21] X. Zhao, C.M. Hayner, M.C. Kung, H.H. Kung, Chem. Commun. 48 (2012) 9909–9911.
[22] M.A. Reddy, B. Breitung, V.S.K. Chakravadhanula, C. Wall, M. Engel, C. Kübel, A.K. Powell, H. Hahn, M. Fichtner, Adv. Energy Mater. 3 (2013) 308–313.
[23] Y. Lu, Z. Wen, J. Jin, X. Wu, K. Rui, Chem. Commun. 50 (2014) 6487–6490.
[24] C. Li, L. Gu, J. Tong, S. Tsukimoto, J. Maier, Adv. Funct. Mater. 21 (2011) 1391–1397.
[25] (a) Y. Makimura, A. Rougier, J.M. Tarascon, Appl. Surf. Sci. 252 (2006) 4587–4592; (b) Y. Makimura, A. Rougier, L. Laffont, M. Womes, J.C. Jumas, J.B. Leriche, J.M. Tarascon, Electrochem. Commun. 8 (2006) 1769–1774.
[26] S. Zhang, Y. Lu, G. Xu, Y. Li, X. Zhang, J. Phys. D. Appl. Phys. 45 (2012) 395301.
[27] X. Fan, J. Shao, X. Xiao, X. Wang, S. Li, H. Ge, L. Chen, Nano Energy 9 (2014) 196–203.
[28] R. Ma, Y. Dong, L. Xi, S. Yang, Z. Lu, C. Chung, Acs Appl. Mater. Inter. 5 (2013) 892–897.
[29] R. Prakash, C. Wall, A.K. Mishra, C. Kübel, M. Ghafari, H. Hahn, M. Fichtner, J. Power Sources 196 (2011) 5936–5944.
[30] R. Prakash, A.K. Mishra, A. Roth, C. Kubel, T. Scherer, M. Ghafari, H. Hahn, M. Fichtner, J. Mater. Chem. 20 (2010) 1871–1876.
[31] K. Rui, Z. Wen, Y. Lu, J. Jin, C. Shen, Adv. Energy Mater. (2014), http://dx.doi.org/10.1002/aenm.201401716.
[32] J.Y. Huang, H. Yasuda, H. Mori, Chem. Phys. Lett. 303 (1999) 130–134.
[33] F. Wang, H.C. Yu, M.H. Chen, L. Wu, N. Pereira, K. Thornton, A. Van der Ven, Y. Zhu, G.G. Amatucci, J. Graetz, Nat. Commun. 3 (2012) 1201.
[34] (a) Y. Zhou, C. Wu, H. Zhang, X. Wu, Z. Fu, Acta Phys. Chim. Sin. 22 (2006) 1111–1115; (b) C. Wall, R. Prakash, C. Kübel, H. Hahn, M. Fichtner, J. Alloys Compd. 530 (2012) 121–126.
[35] R. Ma, M. Wang, P. Tao, Y. Wang, C. Cao, G. Shan, S. Yang, L. Xi, J.C.Y. Chung, Z. Lu, J. Mater. Chem. A 1 (2013) 15060–15067.
[36] (a) M.J. Armstrong, A. Panneerselvam, C. O'Regan, M.A. Morris, J.D. Holmes, J. Mater. Chem. A 1 (2013) 10667–10676; (b) J. Zhou, D. Zhang, X. Zhang, H. Song, X. Chen, Acs Appl. Mater. Inter. 6 (2014) 21223–21229; (c) W. Gu, A. Magasinski, B. Zdyrko, G. Yushin, Adv. Energy Mater. (2014), http://dx.doi.org/10.1002/aenm.201401148.
[37] P. Liao, J. Li, J.R. Dahn, J. Electrochem. Soc. 157 (2010) A355–A361.
[38] F. Cosandey, J.F. Al-Sharab, F. Badway, G.G. Amatucci, P. Stadelmann, Microsc. Microanal. 13 (2007) 87–95.